CrossMark

Journal of
Synchrotron
Radiation

ISSN 1600-5775

Received 16 December 2012
Accepted 6 September 2013

Beamline BL-07 at Indus-2: a facility for microfabrication research

V. P. Dhamgaye,* G. S. Lodha, B. Gowri Sankar and C. Kant

Indus Synchrotrons Utilisation Division, Raja Ramanna Centre for Advanced Technology, Indus-2, Indore, MP 452012, India. *E-mail: vishal@rrcat.gov.in

The X-ray lithography beamline on Indus-2 is now operational, with two modes of operation. With a pair of X-ray mirrors it is possible to tune the energy spectrum between 1 and 20 keV with a controlled spectral bandwidth. In its 'no optics' mode, hard X-rays up to 40 keV are available. Features and performance of the beamline are presented along with some example structures. Structures fabricated include honeycomb structures in PMMA using a stainless steel stencil mask and a compound refractive X-ray lens using a polyimide–gold mask in SU-8.

© 2014 International Union of Crystallography

Keywords: X-ray lithography; beamlines; high-aspect-ratio structures; resist.

1. Introduction

X-ray lithography (XRL) is an established technique for high-aspect-ratio (HAR) microfabrication with sharp side walls and low surface roughness (Ehrfeld & Münchmeyer, 1991). XRL is typically classified according to the energy of the radiation: soft X-ray lithography (SXRL) using 1–3 keV X-ray energies; deep X-ray lithography (DXRL) using X-ray energies up to 20 keV; and ultra-deep X-ray lithography (UDXRL) when X-ray energies greater than 20 keV are used. Many XRL beamlines are operational on synchrotron facilities (Utsumi & Kishimoto, 2005; Romanato *et al.*, 2001) and are used for development of varieties of microstructures. XRL is used for fabrication of compound refractive lenses (Nazmov *et al.*, 2011), submicrometre HAR structures (Achenbach, 2004), anti-scatter grids (Makarova *et al.*, 2003), ultra-thick and ultra-high-aspect-ratio microstructures (Jian *et al.*, 2003) and HAR nanostructures (Kim & Lee, 2008). The device structures fabricated are being used in multiple disciplines such as optical, mechanical, electrical, biological and chemical engineering fields.

The Indus-2 electron synchrotron source presently operates at 2.5 GeV and 100 mA, with significant X-ray flux up to 40 keV (Singh, 2011). A beamline dedicated for soft and deep XRL (BL-07) on Indus-2 has been constructed for undertaking microfabrication research. BL-07 features a special lithographic window covering SXRL, DXRL and UDXRL for development of HAR microstructures. The essential requirement to perform XRL is an X-ray mask. X-ray mask processing technology based on polyimide membrane and gold absorber film is used. This process has the advantage of being low cost, simple to process and compatible with in-house processing technologies. BL-07 is used for fabricating structures in positive resist polymethylmethaacrylate (PMMA) and negative resist SU-8 with an aspect ratio of $\sim$50.

2. Beamline overview

The BL-07 beamline is installed on a 1.5 T bending-magnet source. A schematic layout of the beamline is shown in Fig. 1 (Lodha *et al.*, 2007). The beamline consist of two X-ray mirrors with the corresponding mirror control systems, slits, filters, Be window assemblies and X-ray scanner systems. Beamline optics parameters are calculated at 1.5 keV X-ray energy where high spatial resolution is achieved due to reduced photoelectron blur (Khan *et al.*, 1999). The beamline optics provides an X-ray energy spectrum tuned in the

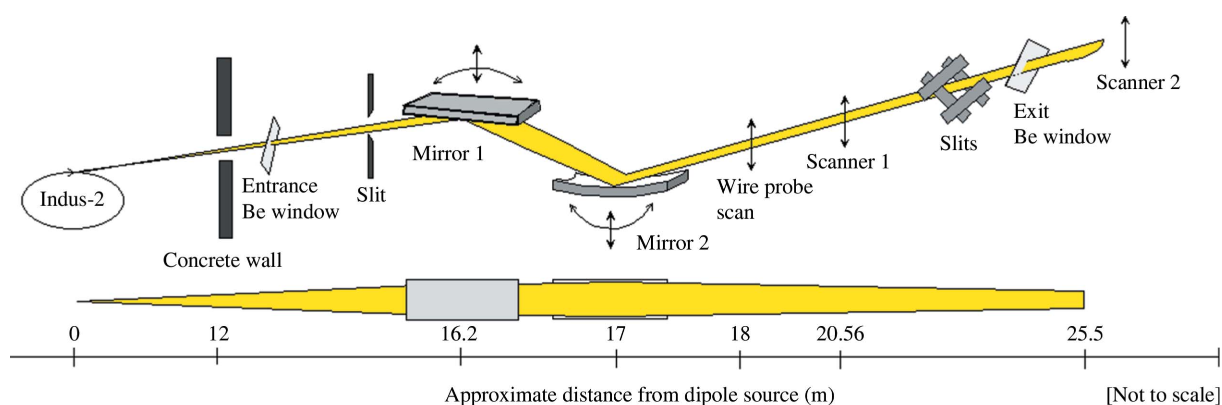

Figure 1
Schematic layout of the XRL (BL-07) beamline.

Table 1
Main parameters of beamline BL-07.

Source	2.5 GeV Indus-2, 1.5 T bending magnet
Source size	σ_y = 232 µm, σ_x = 272 µm
Emittance	58 nm rad with 1% coupling
Length of beamline	25.5 m
Energy range of beamline	1–20 keV with mirrors, >20 keV without mirrors
Reflecting mirrors	Pt-coated Si mirrors (plane and torroidal)
Mirror size	100 mm × 650 mm
Beamline acceptance	5 mrad (H) and 0.62 mrad (V) (3σ at 1.5 keV)
Beam size at sample	55–100 mm (H) × 2–10 mm (V) (depending upon mirror angular settings)
Angular range	0–2°
Filters	Be and Al

1–20 keV energy range with two mirrors and for higher energies (>20 keV) the beamline can be operated without X-ray mirrors. The main parameters of the beamline are summarized in Table 1.

The beamline can be divided into various parts: the front-end inside the storage ring tunnel, the optics hutch, the experimental hutch 1 and the experimental hutch 2. The front-end of the beamline has features to protect the vacuum of the storage ring, define the beam dimensions (Raghuvanshi *et al.*, 2007) and provide beam position information. The front-end of BL-07 consists of a beam absorber, a pair of X-ray beam position monitors, fast-closing shutter and safety shutter. A fast-closing shutter is installed 20 m upstream of the exit Be window to provide vacuum protection of the storage ring within 10 ms if the Be window breaks. This feature is essential for operating the beamline in SXRL mode with a Be window thickness of only 15 µm. A safety shutter is used for absorbing high-energy Bremsstrahlung during entry into the hutches. A water-cooled synchrotron radiation beam absorber is installed before the vacuum gate valves and fast-closing shutter to protect these components from high thermal load.

The optics hutch houses a flat mirror and a toroidal mirror designed to keep the mirror deflected beam parallel to the incident beam. The X-ray mirrors horizontally collimate and vertically focus the synchrotron radiation on the mask–wafer plane of the X-ray scanner in the experimental hutch 2.

The beam is brought into air in experimental hutch 1 to perform the X-ray exposures under atmospheric conditions. Experimental hutch 1 is planned to be used for characterization and testing of X-ray optics and detectors. The main characteristics of the beamline are to provide a wider energy range with high flux and good uniformity in the horizontal plane. The beamline accepts 3σ of bending-magnet source in the vertical direction at 1.5 keV and 5 mrad horizontal divergence to collect the maximum radiated power and yet maintaining the manageable beam channel along the beamline length. Presently, the horizontal divergence is limited to 4 mrad due to the smaller cross-section used for the fixed mask in the beamline front-end but will ultimately be changed to its design goal of 5 mrad.

2.1. Mirror system

The design geometry, positions and angles of the mirrors along the beam are implemented in such a way that the X-ray beam remains parallel to the incident beam and arrives at a fixed height at the end of the beamline. This geometry avoids tilting of the X-ray mask and resist during X-ray exposure. The mirrors system consists of two X-ray mirrors, a plane mirror (M1) and a toroidal mirror (M2). M1 is used as a short-wavelength cut-off reflector and absorbs the synchrotron radiation heat load. The source-to-M2 distance is 17 m and the experimental station in experimental hutch 2 is 8.5 m downstream of mirror M2. The distance between M1 and M2 is 0.8 m. The radius of curvature of M2 is based on the optical parameters calculated at 1.5 keV X-ray energy. The meridional radius is 420 m which focuses the beam in the vertical direction, and the sagittal radius of 0.55 m collimates the beam in the horizontal direction. The beam size changes at the experimental station(s) due to divergence of the beam from the fixed radii of curvature of M2. M1 and M2 mirrors are coated with a Cr/Pt layer with surface roughness of 5 Å and the slope error is ~5 µrad in the meridional direction. Both mirrors are provided with side-cooling arrangements and are housed inside a 2 m-long vacuum chamber. The mirrors are mounted on three point ultra-high-vacuum-compatible linear actuators. The grazing incidence angles of the mirror(s) is set between 0 and 2° with an accuracy of ~5 µrad. The linear actuators provide 1 µm accuracy in vertical positioning for both the mirrors. M2 is translated in the vertical direction with respect to M1 to ensure that the beam falls at the centre position of M2 at various angular settings. The effects of surface figure errors, thermal bump and misalignment errors on the performance of the beamline optical elements are used to determine the beam quality parameters using the beamline design simulation codes *RAY* (Schafers, 2008) and *ShadowVUI* (Sanchez del Rio & Dejus, 1998).

2.2. Experimental stations

Two X-ray scanners are used for conducting X-ray exposure in air, vacuum and He atmosphere. Vertical scanning of the samples (*e.g.* resist, *etc.*) is introduced into the stationary path of the synchrotron radiation beam due to the smaller size of the vertical beam. The scanning is continued until a pre-determined X-ray exposure dose is imparted to the sample. Both X-ray scanners are sequentially arranged and only one scanner can be used at a time (see Fig. 1). Scanner 1 is installed in experimental hutch 1 at a distance of 20.56 m and scanner 2 is installed in experimental hutch 2 at 25.5 m away from source point. Scanner 1 consists of a vertical scanning stage [shown in Fig. 2(*a*)] with the possibility of mounting multiple samples during a single exposure. In this case exposures are performed only in air. With the ease of handling samples in air, samples such as X-ray resist, radiochromic films, chemical solutions and biological samples can be used for X-ray exposures. Scanner 2 consists of a vertical scanning stage, rotation and tilt module, water-cooled mask–wafer stage and water-cooled apertures. A goniometer with rotation arm and tilt stage is moved on two guided vertical scanning stages actuated by two stepping motors operated in synchronized motion. The major parameters of scanner 2 are illustrated in Table 2. The vertical travel range is ±90 mm with the speed controllable between 1 and 30 mm s^{-1}. The variable scanning speed allows for control of the exposure time during single-pass experiments, which is especially useful for reducing the thermal degradation of the resist at higher electron beam current. Fig. 2(*b*) shows an inside view of scanner 2 with an X-ray mask and X-ray-sensitive photoresist in the mounted condition. X-ray masks and wafers up to 100 mm × 100 mm square or circular of diameter 100 mm can easily fit on the mask–wafer mounting assembly. This assembly is rotated over a 360° range and tilted between 0 and 90° for fabrication of non-traditional (three-dimensional) structures. In the case of multiple exposures, alignment marks of the X-ray mask and photoresist are aligned with an accuracy of <5 µm using an offline alignment stage. Recently a high-temperature set-up was added to scanner 2 for maintaining the resist at elevated temperatures. This attachment is used for direct etching of PTFE using synchrotron X-rays. A future upgrade is planned in scanner 2 to introduce moving mask technology (Tabata *et al.*, 2002) for the fabrication of three-dimensional structures.

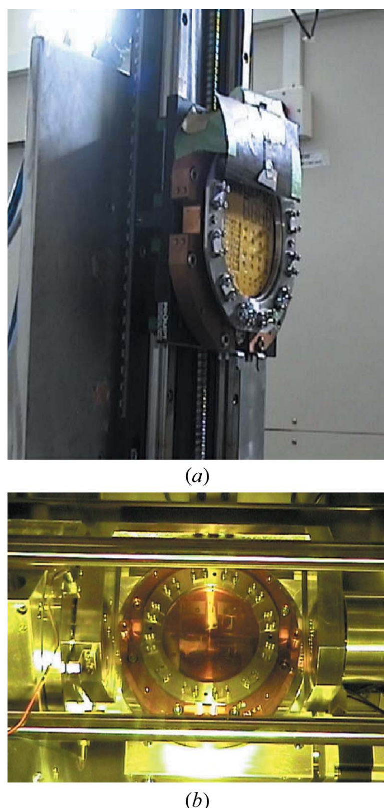

(*a*)

(*b*)

Figure 2
(*a*) Air-based X-ray scanner 1. (*b*) Inside view of X-ray scanner 2 with X-ray mask and resist in the mounted condition.

2.3. Other beamline components

Vacuum-compatible slit systems are used in BL-07. The vertical slits upstream of the mirrors are used to define the vertical acceptance for M1. A four-jaw slit is used to reduce the exposure field in scanner 2. Al (50, 100, 200 µm) and Be (125, 175, 400 µm) filters are used for controlling the dose in PMMA. For diagnostic purposes, the beamline uses X-ray beam position monitors for beam position determination and a fluorescent screen and wire probe scanner for beam profile measurements. Specially designed X-ray beam position monitors (Dhamgaye *et al.*, 2011) are installed in the front-end of this beamline. Vacuum-compatible fluorescent screens coated on copper sheets are installed at two locations (upstream of the mirror system and scanner 2) for visualization of the beam. The positions and profiles of the direct and reflected beam are detected using a 60 µm-diameter gold wire probe installed 18 m from the source point.

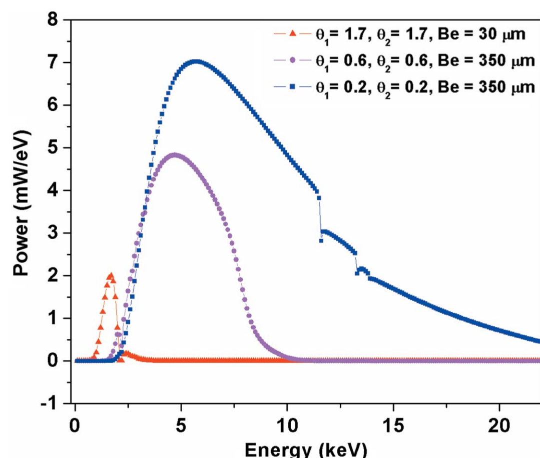

Figure 3
Energy power spectrum for different mirror(s) angular settings available in the mask–wafer plane. The lowest energy spectrum (red triangles) is not available to users due to the thicker Be window assembly.

Table 2
Major parameters of X-ray scanner 2.

Exposure window	±90 mm (V), ±40 mm (H)
Exposure environment	Vacuum, helium and air
Mask–resist size	Circular: 100 mm diameter; square: 100 mm × 100 mm
Resist thickness	1–5000 µm or higher
Mask–wafer tilt and rotation	Tilt 0–90° and rotation ±180°
Gap between mask and resist	0–100 µm
Offline alignment stage	For multiple exposure, alignment accuracy between mask and resist is <5 µm

3. Measured beamline characteristics

Some of the early results of the beamline are reported by Dhamgaye *et al.* (2012). Fig. 3 shows the energy–power spectra for three angular settings of mirrors and Be windows (175 µm or 15 µm). Presently the energy spectrum between 1 and 2 keV is not available for users due to the thicker Be window. In the two-mirror mode of operation, the highest power is available for grazing incidence angles of ∼0.2°. Under typical beamline operating conditions when both the mirrors are set at 0.6°, we obtain a pink energy spectrum between 3 and 10 keV (line with solid purple circles in Fig. 3). It is convenient to characterize the X-ray beam at the scanner 1 mask–wafer plane location and the performance of the beamline can be extended to the scanner 2 mask–wafer plane. A point diagram showing the intensity distribution of the beam in the *xy* plane (*z* is the direction of propagation) at the scanner 1 position simulated using the *RAY* ray-tracing software is shown in Fig. 4(*a*). The size of the beam is 2.5 mm (V) and 70 mm (H). The characteristics smile curve of the image is due to the toroidal mirror shape. The actual beam is recorded using radiochromic film and shown in Fig. 4(*b*) with an area of 2.5 mm (V) and 68 mm (H). A high-quality microstructure with uniform depth on the wafer is dependent on the dose uniformity at the mask–wafer plane. The intensity variation in the horizontal direction is about

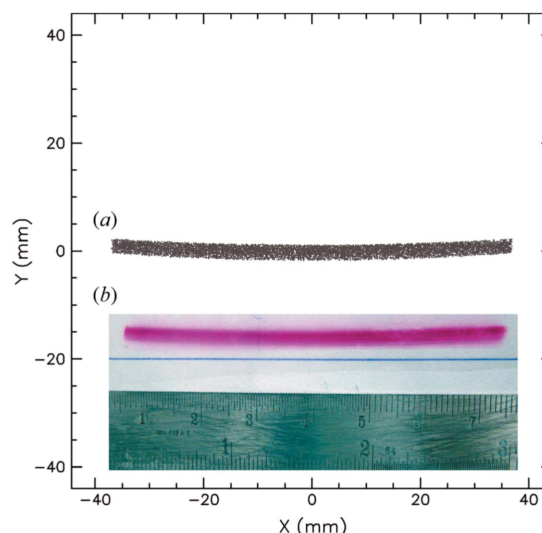

Figure 4
(*a*) Calculated and (*b*) measured intensity distribution in the *xy* plane at X-ray scanner 1.

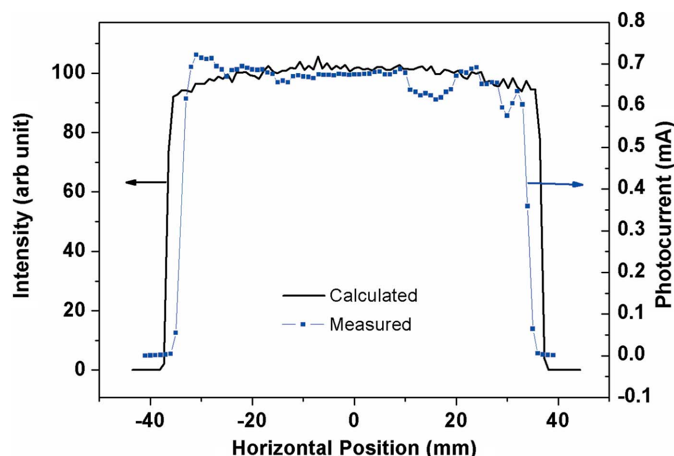

Figure 5
Horizontal intensity distribution of the beam in the mask–wafer plane of scanner 1 calculated using ray-tracing software and corresponding measured intensity.

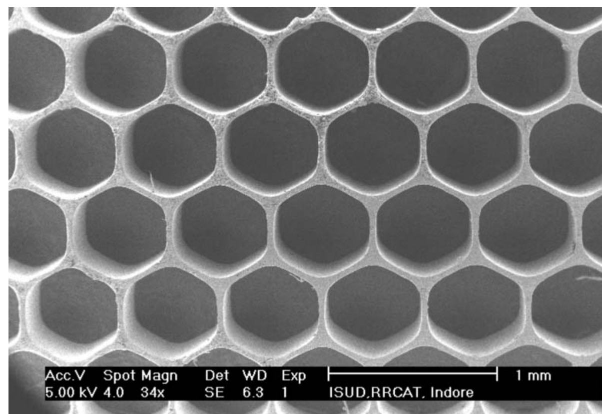

Figure 7
HAR structure of a hexagonal pattern with 40 µm wall thickness with 1000 µm depth fabricated in PMMA.

±12% for the two-toroidal-mirror geometry and was reduced to ±4% using an appropriate X-ray compensation filter (Kaneko *et al.*, 1991). In the present case the calculated horizontal uniform intensity for the two-mirror geometry (3–10 keV spectral band) is found to be ±5%. The horizontal intensity (vertical integrated) uniformity is measured by placing a 1 mm line slit in front of the photodiode and scanning the photodiode in the horizontal direction with incremental steps of 1 mm. The measured and calculated horizontal intensity distribution is shown in Fig. 5. The measured peak variation of intensity in the horizontal direction is ±7%, which is close to the calculated value. The glitches in the horizontal intensity are due to surface figure errors in M2. The higher non-uniformity in the horizontal intensity can also be attributed to heavy-element impurities in the Be foil and to changes in the synchrotron radiation beam position due to electron beam drift inside the storage ring. The vertical beam profile was measured using a wire probe scan. Fig. 6 shows the calculated and measured beam profile at 18 m from the source point. The measured beam profile is in good agreement with the calculated profile curve.

4. X-ray masks and lithographic structures

X-ray masks providing high contrast between exposed and unexposed areas have been developed. These masks include a low-cost stencil mask for poorer resolution (>50 µm) and precision masks using photolithography and gold electro-deposition on polymer membrane. The stencil masks can be fabricated from stainless steel or Cu of 100 µm thicknesses. The high-resolution X-ray mask with SU-8 and polyimide membrane-based gold absorber pattern masks are primarily fabricated for the development of X-ray optical elements.

A typical structure fabricated using a stainless steel X-ray mask in PMMA resist is shown in Fig. 7. The exposure is carried out in a vacuum (10^{-2} mbar) and with an exposure dose of ~55 mA h. The honeycomb patterns have a HAR of 25:1. The same structure is repeated on a 6 mm-thick PMMA sheet with an aspect ratio of 30:1 (minimum feature 100 µm and depth 3000 µm). Compound refractive X-ray lenses in PMMA are fabricated using a polyimide membrane–gold absorber X-ray mask (Dhamgaye & Lodha, 2012). In this case the minimum feature size is 15 µm with an aspect ratio of 54:1. X-ray lenses also fabricated in a single spin-coated layer of SU-8 are shown in Fig. 8 with a relief depth of 500 µm. These lenses are used for micro-focus characterization at Indus-2 between X-ray energies of 8 and 20 keV (Dhamgaye *et al.*, 2013). SU-8 lenses are reported to withstand higher radiation dose without deterioration and are attractive to use in third-generation synchrotron facilities. HAR comb structures are developed in PMMA using BL-07 with possible application in the areas of sensors, energy harvesters, resonators and filters (Shukla *et al.*, 2013).

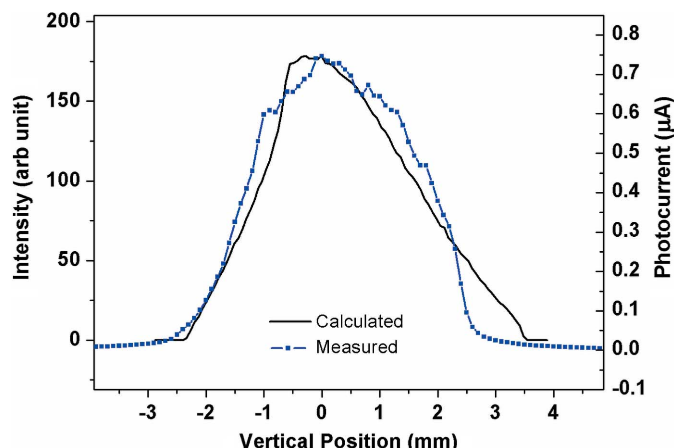

Figure 6
Calculated and measured vertical beam profile by wire probe scan method at a distance of 18.0 m from the source point.

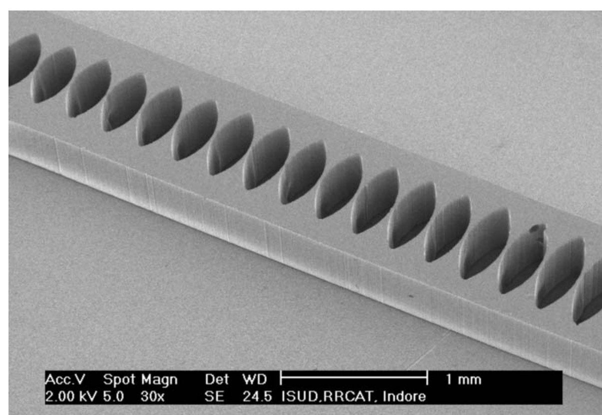

Figure 8
Compound refractive lens fabricated in the high-radiation-resistance material SU-8.

5. Ancillary facilities

We are setting up new facilities around the beamline for efficient utilization of the beamline and for science complimentary to the X-ray lithography activity. An e-beam lithography machine is being installed for high spatial resolution and high density patterned structures, which will be used for the fabrication of X-ray masks. A deep reactive ion etching facility is also installed to fabricate high aspect structures in silicon and metals. Various characterization tools, like a scanning electron microscope, ellipsometer, white-light interferometer, stylus profilometer and Nomarski microscope are available at the centre. A confocal microscope for three-dimensional surface profilometry is being set up. Facilities for Ni, Au, Cu electrodeposition are available for the development of X-ray masks and electroforming of device structures.

6. Facility access

Access to BL-07 and its ancillary facilities are available *via* direct access or joint programmes of collaboration, for short- and long-term project proposals. Users can contact the beamline scientist for initial discussions and to explore the scientific viability of proposed projects. Project proposals are reviewed by the committee for beam time allotment.

7. Conclusions

We have developed and are maintaining the XRL beamline which is the first of its kind in India. The beamline is used for engineering and industrial applications. The wide width and high spectral power of the beam allows for the development of microstructures on a wider area up to 100 mm × 100 mm and for depths up to 3000 μm. X-ray masks have been developed for the first time in India. The capabilities of the X-ray scanner and BL-07 are evaluated by fabrication of multiple types of microstructures. Honeycomb structures are fabricated in PMMA and refractive lenses are developed in SU-8.

Besides the usual utilization of BL-07 for X-ray lithography, it is also used for white-beam experiments like the synthesis of noble nanoparticles (Misra *et al.*, 2013) and radiation physics experiments (Nayak *et al.*, 2012). Initial experiments for direct etching of PTFE show good results and further studies are being carried out. In the future, we would like to adapt the beamline for X-ray optical element and detector testing in white- and monochromatic-light modes.

The authors would like to thank Dr S. K. Deb for help and support. They would also like to thank Dr P. D. Gupta for constant motivation and encouragement. The help from Mrs P. Tiwari in obtaining the SEM image and technical help from Mr B. S. Thakur and Mr M. Nookaraju for beamline operations are gratefully acknowledged.

References

Achenbach, S. (2004). *Microsyst. Technol.* **10**, 493–497.
Dhamgaye, V. P., Gowri Sankar, B., Garg, C. K. & Lodha, G. S. (2012). *AIP Conf. Proc.* **1447**, 527–528.
Dhamgaye, V. P. & Lodha, G. S. (2012). *AIP Conf. Proc.* **1447**, 525–526.
Dhamgaye, V. P., Lodha, G. S. & Kane, S. R. (2011). *Nucl. Instrum. Methods Phy. Res. A*, **659**, 525–527.
Dhamgaye, V. P., Tiwari, M. K., Garg, C. K., Tiwari, P., Sawhney, K. J. S. & Lodha, G. S. (2013). *Microsyst. Technol.* Submitted.
Ehrfeld, W. & Münchmeyer, D. (1991). *Nucl. Instrum. Methods Phys. Res. A*, **303**, 523–531.
Jian, L., Loechel, B., Scheunemann, H., Bednarzik, M., Desta, Y. M. & Goettert, J. (2003). *Proceedings of the International Conference on MEMS, NANO and Smart Systems (ICMENS'03)*, 20–23 July 2003, Banff, Alberta, Canada.
Kaneko, T., Saitoh, Y., Itabashi, S. & Yoshihara, H. (1991). *J. Vac. Sci. Technol. B*, **9**, 3214–3217.
Khan, M., Cerrina, F. & Toyota, E. (1999). *J. Vac. Sci. Technol. B*, **17**, 3433–3438.
Kim, Y. C. & Lee, S. S. (2008). *J. Micromech. Microeng.* **18**, 015006.
Lodha, G. S., Dhamgaye, V. P., Modi, M. H., Nayak, M., Sinha, A. K. & Nandedkar, R. V. (2007). *AIP Conf. Proc.* **879**, 1474–1477.
Makarova, O. V., Tang, C. M., Mancini, D. C., Moldovan, N., Divan, R., Ryding, D. G. & Lee, R. H. (2003). *Microsyst. Technol.* **3**, 395–398.
Misra, N., Biswal, J., Dhamgaye, V. P., Lodha, G. S. & Sabharwal, S. (2013). *Adv. Mater. Lett.* **4**, 458–463.
Nayak, M. K., Sahani, P. K., Khare, M., Sahu, T. K., Haridas, P., Dev, V., Dashora, S., Dhamgaye, V., Haridas, G. & Sarkar, P. K. (2012). *Indian J. Pure Appl. Phys.* **50**, 829–831.
Nazmov, V., Reznikova, E., Mohr, J., Saile, V., Vincze, L., Vekemans, B., Bohic, S. & Somogyi, A. (2011). *J. Micromech. Microeng.* **21**, 015020.
Raghuvanshi, V. K., Dhamgaye, V. P., Singh, A. K. & Nandedkar, R. V. (2007). *AIP Conf. Proc.* **879**, 631–634.
Romanato, F., Fabrizio, E., Di, Vaccari, L., Altissimo, M., Cojoc, D., Businaro, L. & Cabrini, S. (2001). *Microelectron. Eng.* **57–58**, 101–107.
Sanchez del Rio, M. & Dejus, R. J. (1998). *Proc. SPIE*, **3448**, 340–345.
Schafers, F. (2008). *Modern Developments in X-ray and Neutron Optics*, edited by A. Erko, M. Idir, T. Krist and A. G. Michette, pp. 9–41. Berlin/Heidelberg: Springer.
Shukla, R., Dhamgaye, V. P., Jain, V. & Lodha, G. S. (2013). *Microsyst. Technol.* Submitted.
Singh, G., *et al.* (2011). *Proceedings of the Indian Particle Accelerator Conference (InPAC 2011)*, IUAC, Delhi, India.
Tabata, O., You, H., Matsuzuka, N., Yamaji, T., Uemura, S. & Dama, I. (2002). *Microsyst. Technol.* **8**, 93–98.
Utsumi, Y. & Kishimoto, T. (2005). *J. Vac. Sci. Technol. B*, **23**, 2903.